Vacuum 207 (2023) 111572

Contents lists available at ScienceDirect

Vacuum

journal homepage: www.elsevier.com/locate/vacuum

The effect of Bi doping on the thermal conductivity of ZnO and ZnO:Al thin films

Filipe C. Correia [a], Joana M. Ribeiro [a], Armando Ferreira [a], J. Sebastián Reparaz [b], Alejandro R. Goñi [b,c], Torben Boll [d], Adélio Mendes [e], Carlos J. Tavares [a,*]

[a] Centre of Physics of Minho and Porto Universities, University of Minho, 4804-533, Guimarães, Portugal
[b] Institut de Ciència de Materials de Barcelona-CSIC (ICMAB), Esfera UAB, 08193, Bellaterra, Spain
[c] ICREA, Passeig Lluís Companys 23, 08010, Barcelona, Spain
[d] Institute for Applied Materials (IAM) and Karlsruhe Nano Micro Facility (KNMFi), Karlsruhe Institute of Technology (KIT), D-76344, Karlsruhe, Germany
[e] LEPABE, Faculty of Engineering of the University of Porto, Rua Roberto Frias s/n, 4200-465, Porto, Portugal

ARTICLE INFO

Keywords:
Doped zinc oxide films
Thermal conductivity
Frequency domain thermoreflectance
Atom probe tomography

ABSTRACT

The dissipation of heat generation has been one of the largest obstacles in the design of semiconductor devices and reducing the thermal conductivity is vital for improving thermoelectric efficiency. This work focuses on the Bi doping effect on ZnO, and ZnO:Al thin films produced by magnetron sputtering with thickness varying between 500 and 900 nm. The approach introduces Bi ions, a higher mass element, into the ZnO metal-oxide matrix, to hinder phonon-mediated heat conduction and, consequently, reduce thermal conductivity. Atom probe tomography (APT) was employed to survey Bi doping distribution in ZnO:Al:Bi and ZnO:Bi thin films and to study the morphology of the grain boundaries. The thermal properties of the thin films were measured by frequency-domain thermoreflectance. Based on thermal conductivity results, it is concluded that the doping of ZnO films with Al has a significant effect on thermal conductivity, being reduced from 6.0 W m^{-1} K^{-1} in its undoped state to 3.3 W m^{-1} K^{-1} for ZnO with ~3 at.% of Al, mainly due to alloy scattering of phonons in the wurtzite cell. Further doping with Bi contributes to a slight reduction in the thermal conductivity of ZnO:Al.Bi films (2.9 W m^{-1} K^{-1}), due to grain boundary scattering by Bi/Bi_2O_3 phases. This result is understood as the confluence of two counteracting effects. On the one hand, the thermal conductivity of the film decreases because Bi, unlike Al, is segregated to grain boundaries and does not substitute Zn in the wurtzite crystal lattice, which is unequivocally demonstrated by APT results. On the other hand, the simultaneous presence of Al and Bi triggers a morphological change with the film's microstructure becoming more columnar. This change in microstructure from 3D island growth in ZnO:Al and ZnO:Bi to a more regular columnar structure in ZnO:Al,Bi limits further reduction in the thermal conductivity.

1. Introduction

The direct energy conversion between the transport of heat and electric charge based on thermoelectric effects has been a topic of long-standing interest in condensed matter materials science for over half a century [1]. The dissipation of heat generation has been one of the most significant obstacles in the design of semiconductor devices [2–4]. It is possible to control heat propagation by engineering the phononic properties of thermoelectric materials, where phonons are the main heat carriers and materials with low thermal conductivities are desired [3]. An effective strategy to obtain high thermoelectric efficiency is to lower the lattice thermal conductivity [5,6]. *K.B. Spooner* et al. [7] used hybrid density functional theory to demonstrate that reducing the lattice thermal conductivity is vital for improving the thermoelectric efficiency in transparent conducting oxides (TCO).

Zinc oxide is a heteropolar II-VI semiconductor with interesting physical-chemical properties that has drawn attention to several fields of research and applications. It is an interesting choice due to its low cost and relatively low deposition temperature, stability in hydrogen plasma, abundancy as a raw material and non-toxicity [8]. ZnO crystallizes in the hexagonal wurtzite structure and displays an intrinsic low n-type electrical conductivity. This, allied with its high transparency and direct

* Corresponding author.
E-mail address: ctavares@fisica.uminho.pt (C.J. Tavares).

https://doi.org/10.1016/j.vacuum.2022.111572
Received 1 February 2022; Received in revised form 7 September 2022; Accepted 3 October 2022
Available online 9 October 2022

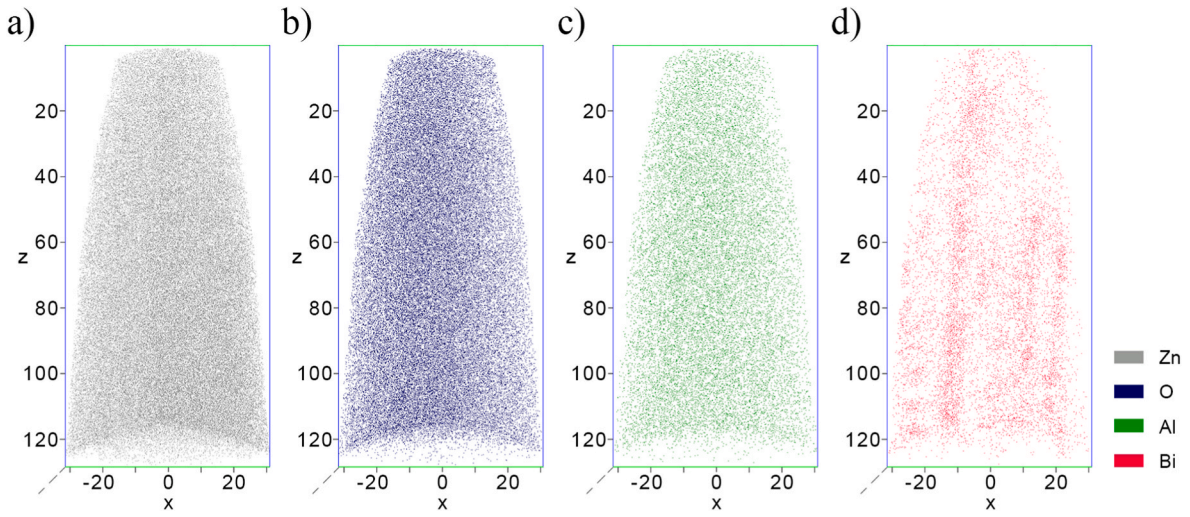

Fig. 1. Side view of the 3D reconstruction obtained by Atom Probe Tomography of a tip of the ZnO:Al,Bi sample with ~1 at.% of Bi. a) Zn content, b) O content, c) Al content, which includes Al and Al_2O_3 species, d) Bi content, which includes Bi and Bi_2O_3 species.

band-gap of ~3.4 eV at room temperature, grants optoelectronic applicability in the near-UV range, such as for photodetectors, light-emitting diodes, photovoltaics, gas sensing and thin-film transistors [9–19], etc. Furthermore, by doping ZnO with Group IIIB elements such as Aluminium (Al), which has n-type carrier concentration, the electrical conductivity can be increased by more than 3-4 orders of magnitude [20–22]. Besides the fact that doped ZnO films are prominent candidates for applications as TCOs, some authors have reported interesting thermoelectric properties as well [23–25]. Bulk ZnO features a thermal conductivity as high as 60 $Wm^{-1}K^{-1}$ that can be lowered with doping or nano-structuring strategies [7,26]. For Al-doped ZnO thin films at room temperature, *T-H. Park* et al. [27] obtained average thermal conductivities in the range of 1.1–5.6 $W\,m^{-1}\,K^{-1}$, while *Loureiro* et al. [28] obtained a thermal conductivity lower than 1.2 $W\,m^{-1}\,K^{-1}$.

In this work, transparent ZnO, ZnO:Bi, ZnO:Al and ZnO:Al,Bi thin films were produced by magnetron sputtering in a confocal geometry. The main objective was to evaluate the effect on the thermal conductivity by the incorporation of Bismuth (Bi) atoms in the ZnO and ZnO:Al wurtzite structure. Since Bi^{3+} is a heavier ion with a very large ionic radius (1.03 Å), in comparison to that of Zn^{2+} (0.60 Å), it is expected that when the former substitutes the latter in the ZnO wurtzite structure it will hinder phonon propagation throughout the lattice. Hence, contributing to the decrease of the thermal conductivity, as reported previously by the authors [25]. Optical pump-probe methods, such as frequency-domain thermoreflectance (FDTR), are well recognized for the measurement the thermal conductivity of thin films. FDTR measures the phase lag of thermally induced oscillations on the surface of a sample with respect to the imposed heat flux from a modulated laser source [4,6]. This technique was used to study the Bi-doping effect on the produced ZnO and ZnO:Al thin films. Due to its unique ability to characterize the 3D morphology and composition of materials, atom probe tomography (APT) was employed to observe the Bi doping content and distribution in ZnO:Al:Bi thin films, as well as to study the morphology of the grain boundaries [29].

2. Materials and methods

Undoped ZnO and doped with Al (~3 at.%) and Bi (~1 at.%) thin films were prepared in a home-made d.c. magnetron sputtering system with thickness varying between 500 and 900 nm. A confocal geometry was used with two circular magnetrons (10 cm diameter) and the following sputtering targets (FHR Anlagenbau GmbH) were used: Bismuth (99.95% purity); ZnO (99.95% purity): ZnO:Al (ZnO 98 wt% Al_2O_3 2 wt %; 99.95% purity). These films were deposited on Si substrates with <100> orientation (SIEGERT WAFER GmbH, Part-No: L14016). The substrates were previously cleaned with isopropanol in an ultrasound bath for 15 min. Before deposition, the substrates were etched in an Ar^+ plasma at 2 Pa to further clean the exposed surfaces. The samples were fixed to a sample holder in the middle of the chamber, radially symmetrical to the centre of the sample holder, fixed at 9 cm (vertically) from the normal to the centre of the targets, in a spinning platform to assure a homogeneous deposition, as previously reported [30]. Several parameters were kept constant throughout all depositions, such as deposition time (30 min), current density on the ZnO and ZnO:Al targets (5.0 mA cm^{-2}), substrate rotation speed (18 rpm), the substrate deposition temperature (200 °C), argon flow (40 sccm), which corresponds to a working pressure of 0.42 Pa, and an isolated substrate bias of −60 V. The vacuum deposition chamber was baked with external sleeves for an hour before the deposition, to reduce the base pressure for each deposition (~10^{-4} Pa). The current density applied to the Bi target (J_{Bi}) to produce the ZnO:Bi and ZNO:Al,Bi films was set to 0.25 mA cm^{-2}.

APT experiments were done at the KNMFi Laboratory for Microscopy and Spectroscopy at the Karlsruhe Institute of Technology, Germany. The thin films were deposited onto a specialized silicon coupon with prefabricated microtips, which were then prepared for APT analysis using a Zeiss Auriga 60 Dual Beam Focused Ion Beam (FIB) in order to obtain a small tip with an apex diameter of 60 nm, containing a roughly 200 nm thick ZnO layer. The tips were measured in a local electrode atom probe (LEAP 4000X HR) in UV-laser mode (30 pJ), with a pulse frequency of 125 kHz, a temperature of 50 K and a detection rate of 0.4%.

The morphology and cross-section of the films studied were investigated by scanning electron microscopy (SEM) with a FEI NOVA 200 FEG equipment operating at a maximum voltage of 30 kV, at SEMAT/UM of the University of Minho.

FDTR experiments were performed at Institut de Ciència de Materials de Barcelona-CSIC. The procedure to measure the thermal properties of the thin films involved the use of two lasers to locally heat (pump, 405 nm) and probe (probe, 532 nm) the temperature at the surface of the film. In order to enhance the thermal sensitivity of the method, a 60 nm thick Au transducer was evaporated onto the surface of the specimens. The output power of the pump laser was modulated in the frequency range between 30 kHz and 20 MHz, which generates thermally induced oscillations of the reflectivity of the sample, leading to a modulation of the reflected power of the continuous wave probe laser. In this way, the phase lag between the heat wave generated by the pump laser and the harmonic response of the sample is sensed against the probe laser by using a lock-in amplifier. The frequency-dependent phase lag is

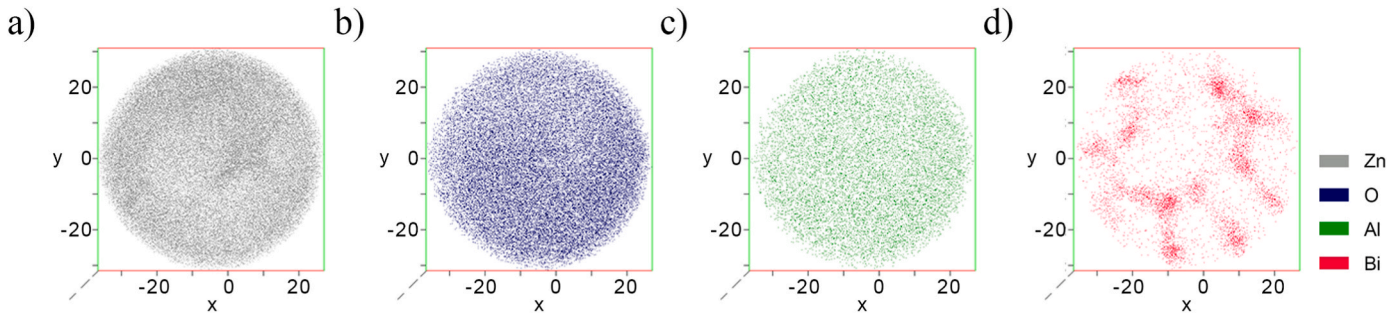

Fig. 2. Top view of the 3D reconstruction obtained by Atom Probe Tomography of a tip of the ZnO:Al,Bi sample with ~1 at.% of Bi, sliced to display the 60–120 nm region in the z-direction. a) Zn content, b) O content, c) Al content, which includes Al and Al_2O_3 species, d) Bi content, which includes Bi and Bi_2O_3 species.

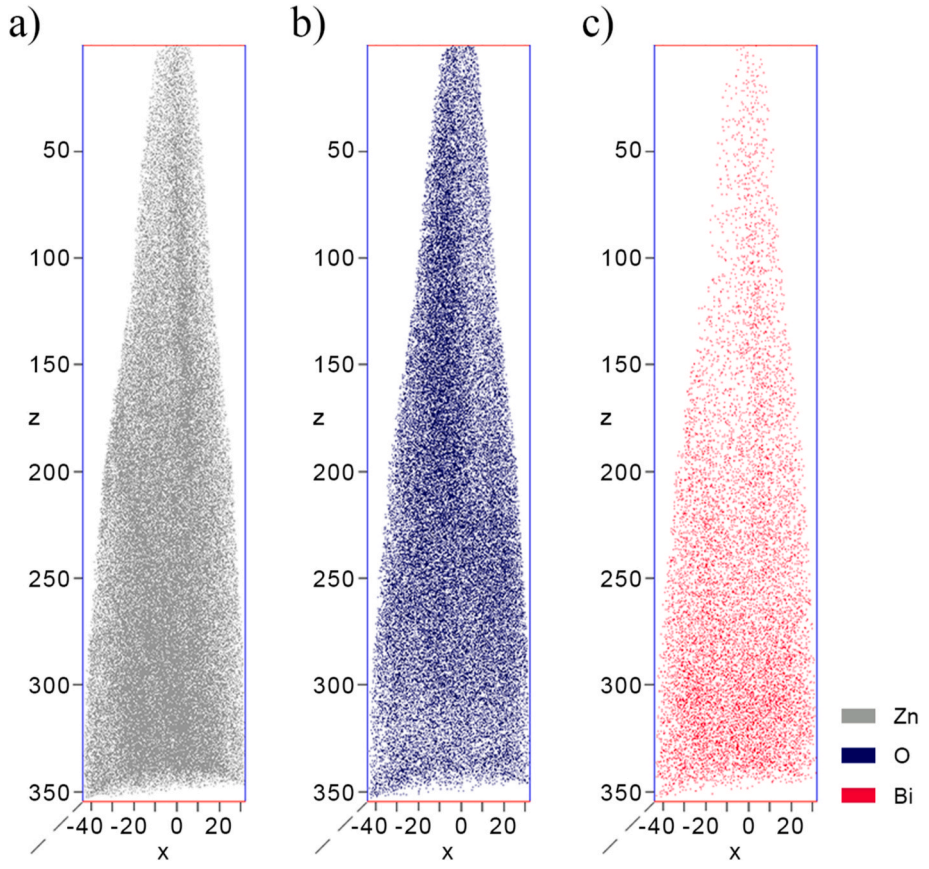

Fig. 3. Side view of the 3D reconstruction obtained by Atom Probe Tomography of a tip of the ZnO:Bi sample with ~1 at.% of Bi.a) Zn content, b) O content, c) Bi content, which includes Bi and Bi_2O_3 species.

modelled numerically, solving the parabolic heat equation for the described geometry. The model used to fit the phase lag curve describes the behaviour of a stack of layers composed by the Au transducer, the undoped and doped ZnO films, the substrate, and an effective thermal boundary conductance that accounts for the two interfaces between the different layers [31,32]. One of the adjustable parameters obtained by least-squares fitting is the out-of-plane thermal conductivity.

3. Results and discussion

Figs. 1 and 2 show the reconstructions of a ZnO:Al:Bi film deposited with approximately ~1 at.% of Bi content, observed laterally and from the top in relation to the film growth direction, respectively. For the top-view (Fig. 2), due to the cone-shape of the APT tip, leading to an apparent inhomogeneity at the center of the reconstruction, the reconstruction was sliced to display the 60–120 nm region in the z-direction. The estimation of the Bi content in the samples is based on a compositional analysis by RBS, XPS and EDX studies on similar films previously published by the authors [30].

In the various side views of the ZnO:Al,Bi sample in Fig. 1, it can be seen that both the matrix elements, Zinc (in grey), Oxygen (in blue), and the Aluminium dopant (in green), are homogeneously distributed throughout the sample. Conversely, the Bi dopant (in red) is more concentrated along three vertical lines. From observing the top views of the same sample (Fig. 2), one can see that both the matrix elements, Zn and O, and the dopant Al, are homogeneously distributed. Again, contrariwise, the distribution of Bi is heterogeneous. From the conjugation of the two views, or rather, the projections of the Bi concentration shown, it is concluded that Bi appears to segregate at the triple points of the grain boundaries and not in all of the boundary surface, as one does

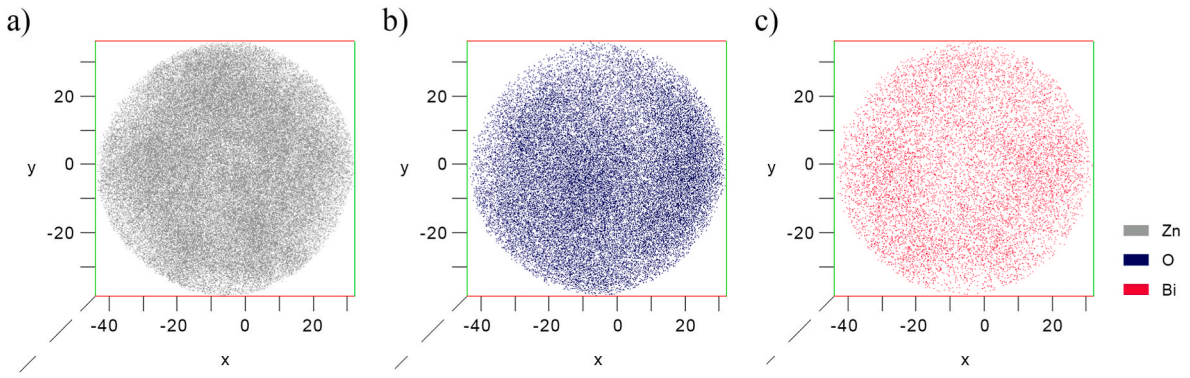

Fig. 4. Top view of the 3D reconstruction obtained by Atom Probe Tomography of a tip of the ZnO:Bi sample with ~1 at.% of Bi, sliced to display the 165–350 nm region in the z-direction. a) Zn content, b) O content, c) Bi content, which includes Bi and Bi_2O_3 species.

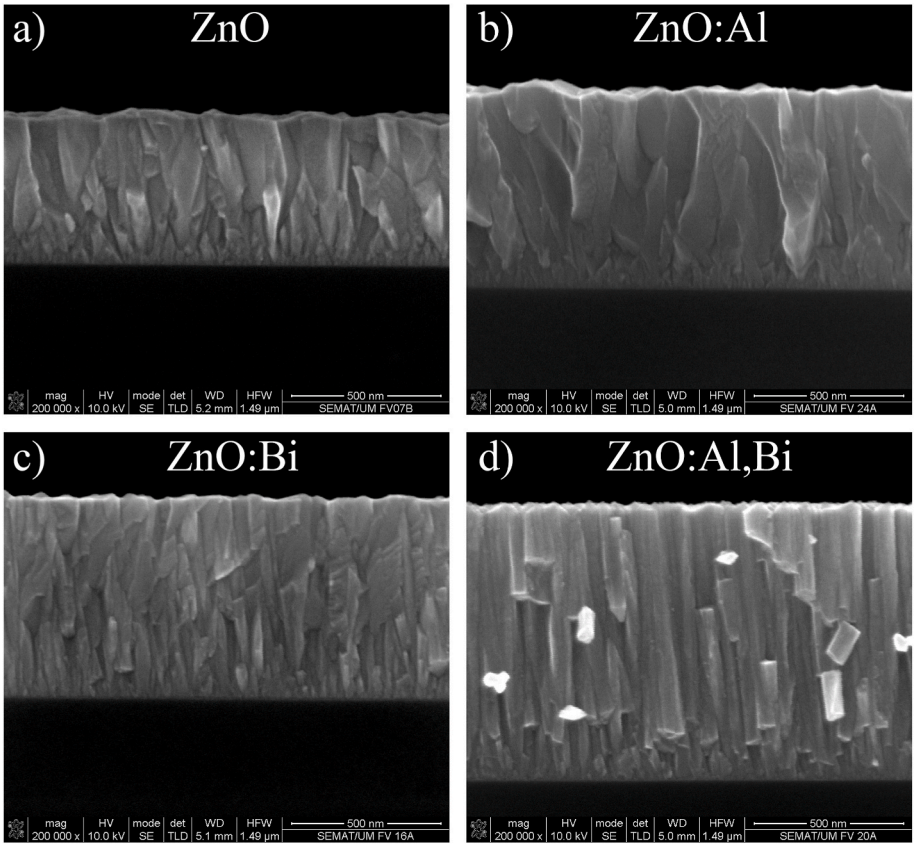

Fig. 5. Scanning electron microscopy cross-sectional micrographs for a) ZnO, b) ZnO:Al, c) ZnO:Bi and d) ZnO:Al,Bi films.

not observe Bi-rich planes but lines. These conclusions are coherent with results already published by the authors [33], according to what was found by transmission electron microscopy (TEM) about very similar samples of ZnO:Ga,Bi. The TEM micrographs in this referred work can be regarded as a sectional analysis according to the xy plane, and coherently with what has been discussed about the APT results, it is possible to conclude that the concentration of Bi is higher at the triple points. This fact reinforces that Bi segregates in the triple points forming small columns, perpendicular to the sample surface. For the case of ZnO:Bi (without Al doping) the APT reconstruction of a sample with ~1 at.% of Bi is shown in Figs. 3 and 4, where the atomic distribution of Zn, O and Bi is homogeneous, hence the segregation of Bi is not observed. Same as before, the top-view (Fig. 4) reconstruction was sliced to display the 165–350 nm region in the z-direction.

From the analysis of the SEM micrographs in Fig. 5 for a) ZnO:Al, b) ZnO:Al,Bi, c) ZnO and d) ZnO:Bi thin films, two conclusions can be made. First, it can be seen that the introduction of Bi in ZnO:Al causes a change in its morphology to a more columnar type. The same is seen in the ZnO samples but in a much less pronounced way. This observation is corroborated by the X-ray diffraction (XRD) results previously published by the authors [25]. Second, the cross-section morphology for ZnO:Al,Bi is more columnar than that of ZnO:Bi. In short, Bi doping seems to promote the columnar growth of the films and is enhanced by the presence of Al. An explanation for why Bi segregation is not observed in the APT topographies for ZnO:Bi films, resides in the fact that ZnO:Al,Bi films are more texturized along [001], when compared to ZnO:Bi, which has a more 3-dimensional growth. Moreover, the triples point are well vertically aligned in ZnO:Al,Bi grains, contrariwise to ZnO:Bi where triple points may not follow a line.

Fig. 6 presents the results of the out-of-plane thermal conductivity

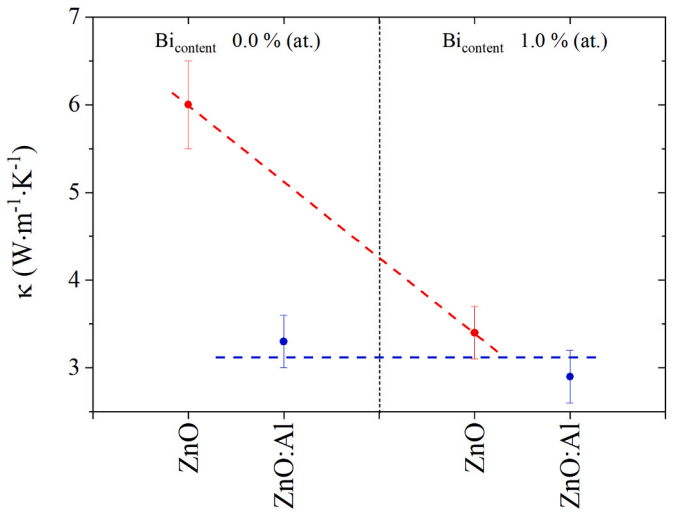

Fig. 6. Total thermal conductivity for the produced ZnO, ZnO:Al, ZnO:Bi and ZnO:Al,Bi films. The error bar represents the deviation in the thermal conductivity estimation from the fits in Fig. 7.

(κ) calculations. The error bar represents the sets of values of κ that produce a fit within an acceptable error margin, as shown in Fig. 7. Bi doping in ZnO promotes a significant decrease in κ, from 6.0 W m^{-1} K^{-1} to 3.4 W m^{-1} K^{-1}, which is not the case with the Bi doping in ZnO:Al films (from 3.3 to 2.9 W m^{-1} K^{-1}, where κ seems unaffected considering the error margin (±0.3 W m^{-1} K^{-1}). Another fact is that ZnO:Al has a lower electrical conductivity when compared to undoped ZnO [25]. It is well known that the thermal conductivity of polycrystalline thin films is always significantly lower compared to that of bulk materials [34]. Moreover, this property depends on film morphology and thickness of the layer, especially for thickness below 1 μm [35,36]. The main origin of this phenomenon is the intense increase in the density of grain boundaries and their respective deterioration and, for smaller film thickness, the surface roughness effects. Thus, for the case of the samples with ZnO matrix, morphological reasons linked to the presence (ZnO:Bi) or absence (ZnO) of Bi/Bi_2O_3 at the triple points of the grain boundaries are sought to justify the κ decrease. As the authors have previously proven that Bi does not enter the ZnO crystal lattice [33], then κ decreases due to the inherent phonon scattering from Bi/Bi_2O_3 at the triple points of the grain boundaries. Curiously, the more pronounced change in morphology from ZnO:Al to ZnO:Al,Bi does not affect significantly κ; albeit reducing by 0.4 W m^{-1} K^{-1}. Alloying ZnO with Al causes a reduction by approximately half of κ due to alloy scattering of the ZnO phonons. Alloying ZnO with Bi causes a similar reduction in κ as for Al. This is at first surprising, because Bi is not incorporated in the ZnO

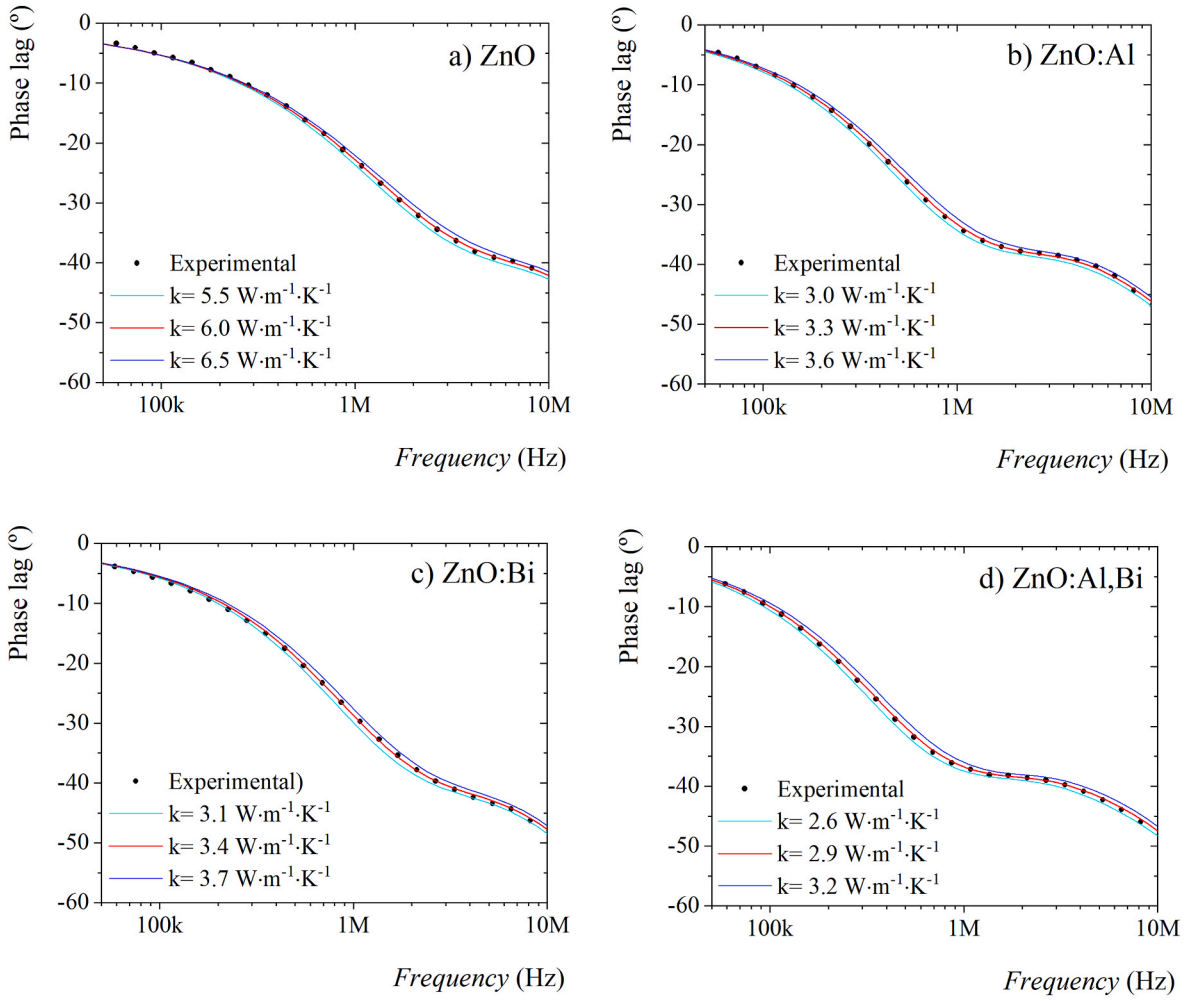

Fig. 7. Frequency-dependent phase lag between the pump (405 nm) and probe (532 nm) lasers for: a) ZnO, b) ZnO:Al, c) ZnO:Bi and d) ZnO:al,Bi films. The central red line corresponds to the considered value for κ in Fig. 6, while the dark and light blue lines correspond to the maximum and minimum values, respectively, for κ considered in the error bars in Fig. 6.

lattice but segregates to the grain boundaries (mainly the triple points). This means that grain boundary scattering is enhanced by Bi incorporation, up to a point of causing a similar effect as alloy scattering with Al in ZnO. There might be a small contribution from the small change in morphology, since the ZnO:Bi film is a bit more columnar than the ZnO:Al one. In the film doped with both Al and Bi, one would expect, at least, another significant reduction of the thermal conductivity. This does not seem to happen and the obvious reason is that there is a clear change in morphology, leading to the enhanced columnar structure. Thus, the change in microstructure from 3D island growth in ZnO:Al and ZnO:Bi to a more regular columnar structure in ZnO:Al,Bi limits further reduction in the thermal conductivity.

4. Conclusions

From APT reconstructions, Zn, O and Al are homogeneously distributed within the crystals (~30 nm), unlike Bi, which was not incorporated into the ZnO wurtzite cell. The Bi distribution is heterogeneous and it segregates at the triple points of the grain boundaries, also inducing the formation of thin columns perpendicular to the surface of the sample in the ZnO:Al,Bi case. Thus, Bi contributes to grain boundary scattering of phonons. A large reduction in thermal conductivity was registered from 6.0 W m^{-1} K^{-1} to 3.3 W m^{-1} K^{-1} upon alloying ZnO with ~3 at.% of Al. Bi doping (~1 at.%) contributes to only a slight reduction in the thermal conductivity of ZnO:Al.Bi films (2.9 W m^{-1} K^{-1}), when compared to that of ZnO:Al films (3.3 W m^{-1} K^{-1}). This means that grain boundary scattering is enhanced by Bi incorporation, up to a point of causing a similar effect as alloy scattering with Al in ZnO. The change in microstructure from 3D island growth in ZnO:Al and ZnO:Bi to a more regular columnar structure in ZnO:Al,Bi limits further reduction in the thermal conductivity.

CRediT authorship contribution statement

Filipe C. Correia: Writing – review & editing, Writing – original draft, Software, Investigation, Data curation. **Joana M. Ribeiro:** Writing – review & editing, Writing – original draft, Investigation, Data curation. **Armando Ferreira:** Writing – review & editing, Funding acquisition. **J. Sebastián Reparaz:** Software, Investigation, Conceptualization. **Alejandro R. Goñi:** Writing – review & editing, Visualization, Validation, Supervision, Resources, Funding acquisition, Formal analysis, Conceptualization. **Torben Boll:** Writing – review & editing, Writing – original draft, Supervision, Software, Resources, Methodology, Investigation, Funding acquisition. **Adélio Mendes:** Supervision, Funding acquisition, Formal analysis. **Carlos J. Tavares:** Writing – review & editing, Writing – original draft, Visualization, Validation, Supervision, Project administration, Methodology, Investigation, Funding acquisition, Formal analysis, Data curation, Conceptualization.

Declaration of competing interest

The authors declare that they have no known competing financial interests or personal relationships that could have appeared to influence the work reported in this paper.

Data availability

Data will be made available on request.

Acknowledgements

Filipe Correia is grateful to the *Fundação para a Ciência e Tecnologia* (FCT, Portugal) for the Ph.D. grant SFRH/BD/111720/2015. Joana Ribeiro is grateful to the FCT, Portugal, for the Ph.D. grant SFRH/BD/147221/2019. Funding is also gratefully acknowledged from FCT/PIDDAC through the Strategic Funds project reference UIDB/04650/2020–2023 and from the Spanish Ministerio de Ciencia e Innovación (MICINN) through grants SEV-2015-0496 (FUNMAT) and CEX2019-000917-S (FUNFUTURE) in the framework of the Spanish Severo Ochoa Centre of Excellence program, and grant PID2020-119777 GB-I00 (THERM2MAIN). This work (proposal ID 2018-020-022469) was carried out with the support of the Karlsruhe Nano Micro Facility (KNMFi, *www.knmf.kit.edu*), a Helmholtz Research Infrastructure at Karlsruhe Institute of Technology (KIT, www.kit.edu).

References

[1] J.R. Sootsman, D.Y. Chung, M.G. Kanatzidis, New and old concepts in thermoelectric materials, Angew. Chem. Int. Ed. 48 (2009) 8616–8639, https://doi.org/10.1002/anie.200900598.
[2] D.U. Kim, K.S. Park, C.B. Jeong, G.H. Kim, K.S. Chang, Quantitative temperature measurement of multi-layered semiconductor devices using spectroscopic thermoreflectance microscopy, Opt Express 24 (2016), 13906, https://doi.org/10.1364/oe.24.013906.
[3] A. El Sachat, F. Alzina, C.M. Sotomayor Torres, E. Chavez-Angel, Heat transport control and thermal characterization of low-dimensional materials: a review, Nanomaterials 11 (2021) 1–32, https://doi.org/10.3390/nano11010175.
[4] M. Rahman, M. Shahzadeh, P. Braeuninger-Weimer, S. Hofmann, O. Hellwig, S. Pisana, Measuring the thermal properties of anisotropic materials using beam-offset frequency domain thermoreflectance, J. Appl. Phys. 123 (2018), https://doi.org/10.1063/1.5033966.
[5] C. Chang, L.-D. Zhao, Anharmoncity and low thermal conductivity in thermoelectrics, Mater. Today Phys. 4 (2018) 50–57, https://doi.org/10.1016/j.mtphys.2018.02.005.
[6] K.T. Regner, S. Majumdar, J.A. Malen, Instrumentation of broadband frequency domain thermoreflectance for measuring thermal conductivity accumulation functions, Rev. Sci. Instrum. 84 (2013) 6–8, https://doi.org/10.1063/1.4808055.
[7] K.B. Spooner, A.M. Ganose, D.O. Scanlon, Assessing the limitations of transparent conducting oxides as thermoelectrics, J. Mater. Chem. (2020), https://doi.org/10.1039/d0ta02247k.
[8] G.J. Exarhos, X.-D. Zhou, Discovery-based design of transparent conducting oxide films, Thin Solid Films 515 (2007) 7025–7052, https://doi.org/10.1016/j.tsf.2007.03.014.
[9] M. Al-Fandi, R. Oweis, B.A. Albiss, T. AlZoubi, M.-A. Al-Akhras, H. Qutaish, H. Khwailah, S. Al-Hattami, E. Al-Shawwa, A prototype ultraviolet light sensor based on ZnO nanoparticles/graphene oxide nanocomposite using low temperature hydrothermal method, IOP Conf. Ser. Mater. Sci. Eng. 92 (2015), 012009, https://doi.org/10.1088/1757-899X/92/1/012009.
[10] A. Janotti, C.G. Van de Walle, Fundamentals of zinc oxide as a semiconductor, Rep. Prog. Phys. 72 (2009), 126501, https://doi.org/10.1088/0034-4885/72/12/126501.
[11] C. Klingshirn, J. Fallert, H. Zhou, J. Sartor, C. Thiele, F. Maier-Flaig, D. Schneider, H. Kalt, 65 years of ZnO research - old and very recent results, Phys. Status Solidi Basic Res. 247 (2010) 1424–1447, https://doi.org/10.1002/pssb.200983195.
[12] Ü. Özgür, Y.I. Alivov, C. Liu, A. Teke, M.A. Reshchikov, S. Doğan, V. Avrutin, S. J. Cho, H. Morko, A comprehensive review of ZnO materials and devices, J. Appl. Phys. 98 (2005) 1–103, https://doi.org/10.1063/1.1992666.
[13] T. Tynell, M. Karppinen, Atomic layer deposition of ZnO: a review, Semicond. Sci. Technol. 29 (2014), 043001, https://doi.org/10.1088/0268-1242/29/4/043001.
[14] K. Ellmer, A. Bikowski, Intrinsic and extrinsic doping of ZnO and ZnO alloys, J. Phys. D Appl. Phys. 49 (2016) 413002, https://doi.org/10.1088/0022-3727/49/41/413002, 413002.
[15] H. Chen, Y. Liu, C. Xie, J. Wu, D. Zeng, Y. Liao, A comparative study on UV light activated porous TiO2and ZnO film sensors for gas sensing at room temperature, Ceram. Int. 38 (2012) 503–509, https://doi.org/10.1016/j.ceramint.2011.07.035.
[16] N.J. Dayan, S.R. Sainkar, R.N. Karekar, R.C. Aiyer, Formulation and characterization of ZnO:Sb thick-film gas sensors, Thin Solid Films 325 (1998) 254–258, https://doi.org/10.1016/S0040-6090(98)00501-X.
[17] A. Moezzi, A.M. McDonagh, M.B. Cortie, Zinc oxide particles: synthesis, properties and applications, Chem. Eng. J. 185–186 (2012) 1–22, https://doi.org/10.1016/j.cej.2012.01.076.
[18] M. Lorenz, M.S. Ramachandra Rao, T. Venkatesan, E. Fortunato, P. Barquinha, R. Branquinho, D. Salgueiro, R. Martins, E. Carlos, A. Liu, F.K. Shan, M. Grundmann, H. Boschker, J. Mukherjee, M. Priyadarshini, N. DasGupta, D. J. Rogers, F.H. Teherani, E.V. Sandana, P. Bove, K. Rietwyk, A. Zaban, A. Veziridis, A. Weidenkaff, M. Muralidhar, M. Murakami, S. Abel, J. Fompeyrine, J. Zuniga-Perez, R. Ramesh, N.A. Spaldin, S. Ostanin, V. Borisov, I. Mertig, V. Lazenka, G. Srinivasan, W. Prellier, M. Uchida, M. Kawasaki, R. Pentcheva, P. Gegenwart, F. Miletto Granozio, J. Fontcuberta, N. Pryds, The 2016 oxide electronic materials and oxide interfaces roadmap, J. Phys. D Appl. Phys. 49 (2016), 433001, https://doi.org/10.1088/0022-3727/49/43/433001.
[19] K.M. Sandeep, S. Bhat, S.M. Dharmaprakash, Structural, optical, and LED characteristics of ZnO and Al doped ZnO thin films, J. Phys. Chem. Solid. 104 (2017) 36–44, https://doi.org/10.1016/j.jpcs.2017.01.003.
[20] T. Yamada, A. Miyake, S. Kishimoto, H. Makino, N. Yamamoto, T. Yamamoto, Low resistivity Ga-doped ZnO thin films of less than 100 nm thickness prepared by ion plating with direct current arc discharge, Appl. Phys. Lett. 91 (2007) 1–4, https://doi.org/10.1063/1.2767213.

[21] F. Wu, L. Fang, Y.J. Pan, K. Zhou, L.P. Peng, Q.L. Huang, C.Y. Kong, Seebeck and magnetoresistive effects of Ga-doped ZnO thin films prepared by RF magnetron sputtering, Appl. Surf. Sci. 255 (2009) 8855–8859, https://doi.org/10.1016/j.apsusc.2009.06.076.

[22] J.N. Duenow, T.A. Gessert, D.M. Wood, B. Egaas, R. Noufi, T.J. Coutts, Investigation of ZnO:Al doping level and deposition temperature effects on CIGS solar cell performance, MRS Proc 1012 (2007).

[23] N. Vogel-Schäuble, Y.E. Romanyuk, S. Yoon, K.J. Saji, S. Populoh, S. Pokrant, M. H. Aguirre, A. Weidenkaff, Thermoelectric properties of nanostructured Al-substituted ZnO thin films, Thin Solid Films 520 (2012) 6869–6875, https://doi.org/10.1016/j.tsf.2012.07.046.

[24] P. Mele, S. Saini, H. Honda, K. Matsumoto, K. Miyazaki, H. Hagino, a. Ichinose, Effect of substrate on thermoelectric properties of Al-doped ZnO thin films, Appl. Phys. Lett. 102 (2013), 253903, https://doi.org/10.1063/1.4812401.

[25] F.C. Correia, P.B. Salvador, J.M. Ribeiro, A. Mendes, C.J. Tavares, Effect on the electrical and morphological properties of Bi incorporation into ZnO:Ga and ZnO:Al thin films deposited by confocal magnetron sputtering, Vacuum 152 (2018) 252–260, https://doi.org/10.1016/j.vacuum.2018.03.033.

[26] M. Ruoho, K. Valset, T. Finstad, I. Tittonen, Measurement of thin film thermal conductivity using the laser flash method, Nanotechnology 26 (2015), 195706, https://doi.org/10.1088/0957-4484/26/19/195706.

[27] T.H. Park, N.W. Park, J. Kim, W.Y. Lee, J.H. Koh, S.K. Lee, Cross-plane temperature-dependent thermal conductivity of Al-doped zinc oxide thin films, J. Alloys Compd. 638 (2015) 83–87, https://doi.org/10.1016/j.jallcom.2015.03.065.

[28] J. Loureiro, N. Neves, R. Barros, T. Mateus, R. Santos, S. Filonovich, S. Reparaz, C. M. Sotomayor-Torres, F. Wyczisk, L. Divay, R. Martins, I. Ferreira, Transparent aluminium zinc oxide thin films with enhanced thermoelectric properties, J. Mater. Chem. A. 2 (2014) 6649, https://doi.org/10.1039/c3ta15052f.

[29] Y. Yu, C. Zhou, S. Zhang, M. Zhu, M. Wuttig, C. Scheu, D. Raabe, G.J. Snyder, B. Gault, O. Cojocaru-Mirédin, Revealing nano-chemistry at lattice defects in thermoelectric materials using atom probe tomography, Mater. Today 32 (2020) 260–274, https://doi.org/10.1016/j.mattod.2019.11.010.

[30] J.M. Ribeiro, F.C. Correia, P.B. Salvador, L. Rebouta, L.C. Alves, E. Alves, N. P. Barradas, A. Mendes, C.J. Tavares, Compositional analysis by RBS, XPS and EDX of ZnO:Al,Bi and ZnO:Ga,Bi thin films deposited by d.c. magnetron sputtering, Vacuum 161 (2019) 268–275, https://doi.org/10.1016/j.vacuum.2018.12.038.

[31] A.J. Schmidt, R. Cheaito, M. Chiesa, A frequency-domain thermoreflectance method for the characterization of thermal properties, Rev. Sci. Instrum. 80 (2009), https://doi.org/10.1063/1.3212673.

[32] M. Yoshiizumi, N. Oikawa, K. Shimada, S. Endo, M. Sugiyama, H. Mikami, R. Maeda, T. Hayakawa, Thermal conductivity evaluation of polymer thin film, Trans. Mater. Res. Soc. Japan. 38 (2014) 555–559, https://doi.org/10.14723/tmrsj.38.555.

[33] F.C. Correia, J.M. Ribeiro, A. Kuzmin, I. Pudza, A. Kalinko, E. Welter, A. Mendes, J. Rodrigues, N. Ben Sedrine, T. Monteiro, M.R. Correia, C.J. Tavares, The role of Ga and Bi doping on the local structure of transparent zinc oxide thin films, J. Alloys Compd. 870 (2021), 159489, https://doi.org/10.1016/j.jallcom.2021.159489.

[34] H. Hosono, K. Ueda, Transparent conductive oxides, in: S. Kasap, P. Capper (Eds.), Springer Handb. Electron. Photonic Mater., Springer International Publishing, Cham, 2017, p. 1, https://doi.org/10.1007/978-3-319-48933-9_58.

[35] S.S. Shinde, C.H. Bhosale, K.Y. Rajpure, Structural, optical, electrical and thermal properties of zinc oxide thin films by chemical spray pyrolysis, J. Mol. Struct. 1021 (2012) 123–129, https://doi.org/10.1016/J.MOLSTRUC.2012.04.045.

[36] Y. Xu, M. Goto, R. Kato, Y. Tanaka, Y. Kagawa, Thermal conductivity of ZnO thin film produced by reactive sputtering, J. Appl. Phys. 111 (2012), https://doi.org/10.1063/1.4706569.